

Hydroelastic analysis of a truss pontoon Mobile Offshore Base

S. Somansundar^{1a}, R. Panneer Selvam^{*1} and D. Karmakar^{2b}

¹Department of Ocean Engineering, Indian Institute of Technology Madras,
Chennai – 600036, Tamil Nadu, India

²Department of Applied Mechanics and Hydraulics, National Institute of Technology Karnataka,
Surathkal, Mangalore – 575025, India

(Received September 30, 2018, Revised October 10, 2019, Accepted October 12, 2019)

Abstract. Very Large Floating Structures (VLFS) are one among the solution to pursue an environmentally friendly and sustainable technology in birthing land from the sea. VLFS are extra-large in size and mostly extra-long in span. VLFS may be classified into two broad categories, namely the pontoon type and semi-submersible type. The pontoon-type VLFS is a flat box structure floating on the sea surface and suitable in regions with lower sea state. The semi-submersible VLFS has a deck raised above the sea level and supported by columns which are connected to submerged pontoons and are subjected to less wave forces. These structures are very flexible compared to other kinds of offshore structures, and its elastic deformations are more important than their rigid body motions. This paper presents hydroelastic analysis carried out on an innovative VLFS called truss pontoon Mobile Offshore Base (MOB) platform concept proposed by Srinivasan and Sundaravadivelu (2013). The truss pontoon MOB is modelled and hydroelastic analysis is carried out using HYDRAN-XR* for regular 0° waves heading angle. Results are presented for variation of added mass and damping coefficients, diffraction and wave excitation forces, RAOs for translational, rotation and deformational modes and vertical displacement at salient sections with respect to wave periods.

Keywords: Hydroelasticity; Mobile Offshore Base (MOB); Hydrodynamic coefficient; fluid forces; Response amplitude operator; vertical displacement; longitudinal and bending stresses

1. Introduction

Population growth in the coastal areas demands vast spaces for their use. Floating platforms concepts have been introduced and are constructed in different parts of the world and these are used as runways, hotels, bridges, heliport etc. near and midst of sea. Such floating structure comes under the category of Very Large Floating Structures (VLFS). It is a technology that allows the artificial land to float on rising sea level and has a minimal effect on marine habitats, water quality, and tidal and natural current flows.

VLFS are floating structures characterized by large length to draft ratios and are flexible, exhibiting elastic responses. VLFS structures falls in two categories namely the pontoon type and

*Corresponding author, Professor, E-mail: pselvam@iitm.ac.in

^a Ph.D. Student, E-mail: somudce@gmail.com

^b Assistant Professor, E-mail: dkarmakar@nitk.edu.in

semi-submersible type and each type have their own pros and cons. The mobile offshore base (MOB) platform is a VLFS with interconnected modules. It has potential applications in shallow to deep ocean waters and can serve as an alternative to existing land bases for operations by the military, such as delivery of critical tactical equipment, personnel and amenities. For the operation in deep waters and ease of mobility, a multi-module design is favourable in which the modules are designed and fabricated in shipyard. The MOB consists of relatively conventional semisubmersible modules which are joined by mechanical connectors and are transported through sea. The mega-float is simple box-type pontoon structures having conventional design and fabricated in the shipyard with small modules. In all of the above mentioned structures the hydroelastic behaviors are more important due to large length to depth ratio (ISSC 2006). The different applications of VLFS include floating airports facilities, Mobile Offshore Base (MOB) for military operations, offshore port facilities, offshore storage and waste disposal facilities, Energy Island and food production habitats (floating cities) etc. Mega floating structures are constructed and have been successfully used around the world. Some of the existing VLFS are listed below (Wang 2015).

- *British Columbia -King pacific lodge princess royal island,*
- *Japan - Brazilian Petrobras P-51, semi-submersible oil platform at operational water depth 1700m, Okinawa Marine Exposition Aqua polis at Hiroshima, Pontoon type Mega-float: floating runway test model, Floating runway at Tokyo airport Haneda, floating restaurant in Yokohama, floating pre-stressed concrete pier at Ujina port, Hiroshima, floating rescue emergency bases located at Tokyo Bay (made of steel), Osaka Bay (Reinforced, floating oil storage bases located at Shirashima,*
- *Hong Kong -Jumbo restaurant,*
- *Netherland -pontoon type floating bridge, floating Road, Hedel,*
- *Singapore- world's largest floating performance stage at Marina Bay,*
- *Norway -Bergsoysund Bridge, built in 1992 near Kristiansund over a fjord, Nordhordland Bridge, built in 1994 at Salhus over a fjord,*
- *USA - floating bridge LaceyV.Murrow Memorial Bridge, Washington Lake, Seattle-mercere (completed 1993).*

Numerical and experimental investigations are essential part of any development and implementation of a VLFS structure. Bishop and Price (1976, 1986) examined a large floating body like VLFS based on Wet and Dry modes. In wet modes, the modal shapes and frequencies are obtained from hull and hydrostatic restoring forces. In dry modes, body is treated as a free-free beam and fluid forces are applied on the dry part of the body. In most of the offshore structures geometrical symmetrical body is widely used. The symmetric structures results in computational reduction. Wu *et al.* (1993) used double composite singularity distribution method (DCSD) to compute the potential flow around and the hydroelastic behavior of very large, flexible structure in waves. Numerical calculations were carried over a quarter of the body's wetted surface, and hence a major reduction in computational requirement is achieved. Lee and Webster (1994) presented the details of fabricating a hydroelastic model of a floating airport to a 1:500 scale with suitable materials and a scheme to measure its motion. The requirement of the modulus of elasticity was about 5-200Mpa and it was suggested that the flexible PVC and polystyrene foam sheets materials are mostly favourable to fabricate hydroelastic models. Zueck *et al.* (1998) examined the development of different structural concepts for MOB platform that provides a forward-deployable logistics facility capable of conducting flight operations, maintenance, and other military

operations. This MOB is intended to cater for the Navy for mission requirements such as conventional take-off and landing of fixed-wing cargo aircraft at sea, cargo transfer to ships and landing craft in open oceans, occupancy of large military personnel during storms, hurricanes and typhoons, large volume storage of a variety of military cargo, long term station keeping in deep water etc. The hydroelastic scaling laws are analytically developed and discussed by Tulin (1999), with emphasis on MOB. Scaling laws for rigid bodies and hinges are included in the analysis. Liu *et al.* (2000) developed four-node quadrilateral shell element using a linear first order shear deformation theory. The results showed that these elements perform well in both moderately thick and thin plates, and it is free of shear locking. Venkataraman (2001) developed (linear and nonlinear) hydrodynamic and hydroelastic computer models for the analysis of MOB for multi-module scale model including connector dynamics. Higher response range was observed in the four module case compared to the single and two module configurations. Pinkster *et al.* (2001) investigated the behavior of an air-supported concept of a large floating structure using model tests and computations based on three dimensional potential theory. He concluded that the still water resistance of air cushion MOB was strongly dependent on the draft and hence in order to attain a high transit speed the lowest possible draft should be maintained. Midship bending moments were found to be significantly reduced by the air cushion. Barrientos *et al.* (2004) developed a coupled finite/boundary element method for free vibration modes of an elastic structure. The influence of fluid is to be taken into the account through added mass formulation, which is posed in terms of boundary integral equations. Linear continuous elements were used to discretize the solid displacements and fluid-solid interface variables.

A new, mapping and interpolation techniques were proposed by Huang and Riggs (2005) for fluid-structure interaction applications. Significant contributions Riggs *et al.* (1998, 1999, 2007, and 2008) on VLFS analysis can be seen in the literature. Suzuki *et al.* (1996) presented an analytical approach based on uniform beam on an elastic foundation to predict hydroelastic behaviour of the VLFS. Kim *et al.* (2007) discussed about bending moment and shear forces at unit connections of VLFS using hydroelastic and rigid body analysis under wave loads. The responses were calculated using higher-order boundary element method (HOBEM) and finite element methods for fluid and structural analysis. Bending moments and shear forces at the connections were obtained from the dynamic equilibrium condition for pressures and inertia forces. Srinivasan *et al.* (2006) presented design analysis of a truss pontoon semi-submersible concept that can be used in deep water. Heave plates attached at the ends of the truss contributed to additional added mass and damping and affected its response. The concept of truss spar was extended to VLFS by Srinivasan and Sundaravadivelu (2013) is called truss pontoon MOB. The critical problem in VLFS is the longitudinal bending moment in waves/current environment and many of the present available VLFS designs are not suitable in hostile ocean. To overcome this, a strong deck and strong longitudinal beams are provided to resist bending moment of the vessel for the survival, standby and operational conditions of the wave. Heavy shell type pontoon is replaced by a simple open frame truss structure and connects the columns just above the keel tank top. This feature reduces the wave exciting forces and consequently the heave motions and the vertical acceleration. The concept of truss pontoon MOB is relatively new and hydroelastic analysis of this structure in waves has not been carried out based on the literature review to date. This paper presents study details on hydroelastic numerical investigation of truss pontoon MOB using HYDroelastic Response ANALysis (HYDRAN).

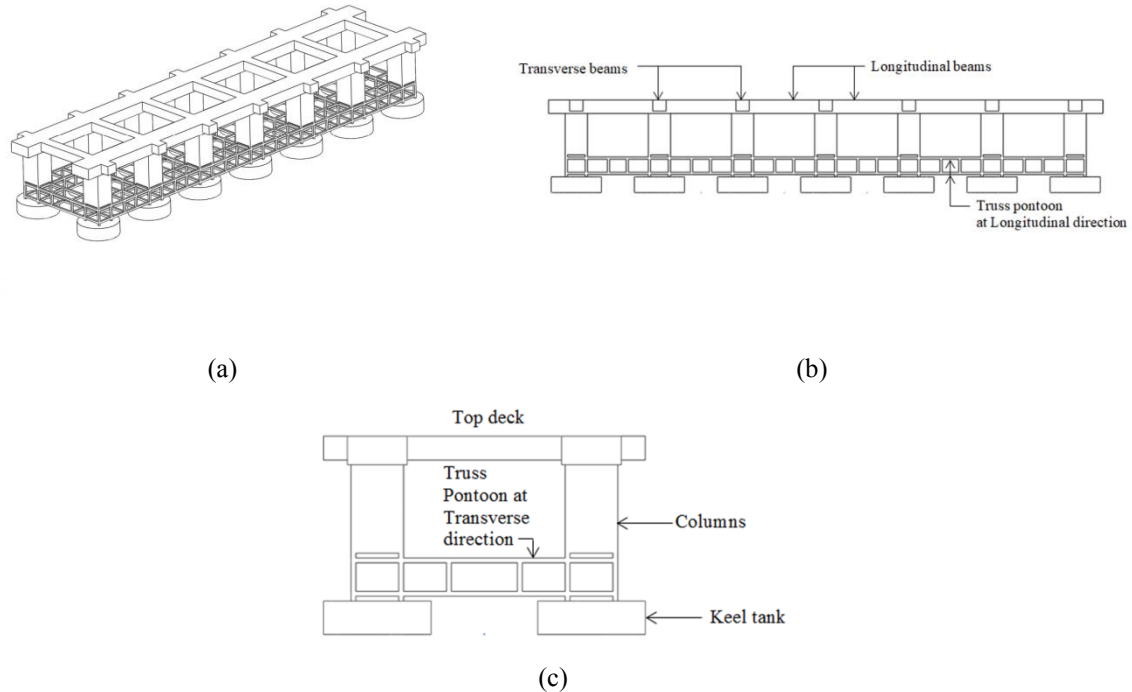


Fig. 1 View of truss pontoon MOB (a) Isometric view, (b) Longitudinal and (c) Cross sectional view of truss

2. Truss pontoon Mobile Offshore Base (MOB)

Truss pontoon MOB, falls under Semi-submersible type VLFS, is a new concept proposed by Srinivasan *et al.* (2013). A schematic view of this concept of a single module is shown in Fig. 1. A single module consists of a main deck supported on two parallel longitudinal beams and series of transverse beams. Columns with circular keel tank at the bottom are attached to the two parallel longitudinal beams. A simple truss frame structure connects the columns at the submerged portion above the keel tank top which is designed to resist axial forces between the columns. Detailed description, behaviour and salient design aspects are dealt by the inventor Srinivasan and Sundaravadivelu (2013). The geometric, mass, hydrostatic, floating stability properties and other details are presented in Table 1. Each module is 500 m long and 135 m wide. The total height is 83 m (approximately) and operational draft is 61.42 m. A single module consists of 19 truss pontoons and 14 deep drafted columns, in two parallel rows. Each column has a circular keel tank attached to its bottom. The rectangular size of the column is 22×20 m and the diameter of the keel tank is 45 m. The deck is supported by means transverse and longitudinal deck beams which can be girder type or any other sections. It has significant less underwater surface area subject to wave forces in the vertical and horizontal directions. Modules are connected in such way so as to reduce span moment resistance of the MOB platform. The transverse beam helps to reduce the longitudinal stress and act as shear load transfer structure. The circular keel tank attached to the deep drafted columns is ballasted by water or by any suitable material as needed by the stability requirements. The structure is towed to the site in un-ballasted condition; they are then ballasted so that the keel

tanks are far below the water surface wherein the wave actions are minimal. The columns provide hydrostatic stability against overturning. Each individual column of the truss pontoon MOB platform is designed with heave period over 22 s (seconds), so that minimum hydrodynamic-motion characteristics for the waves are ensured (2013). Thus the overall truss pontoon MOB platform has almost the same vertical motion characteristics as the individual columns. The truss pontoon MOB platform properties for a single module are presented in Table 1. The truss pontoon MOB platform is designed with minimum heave for the extreme storm unlike the conventional column stabilized semisubmersible unit with the conventional pontoon. The elastic material properties and mass properties of the Truss pontoon MOB are shown in Table 2. The sides of the hull and truss elements in truss pontoon are massless plates. The centre of gravity of the structure is 27.05 m below the still water line and displacement is 628300tonne.

Table 1 Truss pontoon MOB platform properties for a single module

Description	Value	Unit	Description	Value	Unit
Deck			Longitudinal beam		
Length	500	meter	Breadth	25	meter
Breadth	135	meter	Depth	12	meter
Deck Pay load	140000	tonne	Transverse Beam		
Column			Breadth	12	meter
Length	20	meter	Depth	10	meter
Breadth	22	meter	Pontoon long. & transverse members (tubular sections)	3.2m sq. or diameter	meter
Depth	57	meter	Total weight of structures	165190	tonne
Longitudinal spacing c/c	75	meter	Displacement	628300	tonne
Transverse spacing c/c	90	meter	Roll Moment of inertia (I_{xx})	2.0649×10^{12}	kg-m ²
No. columns	14		Pitch Moment of inertia (I_{yy})	1.4704×10^{13}	kg-m ²
Draft	61.42	meter	Yaw Moment of inertia (I_{zz})	1.51158×10^{13}	kg-m ²
Free Board	23	meter	KG	34.37	meter
Total depth	83	meter	Heave period	26.91	s
Keel tank			Pitch period	27.42	s
Diameter of tank	45	meter	Roll period	47.98	s
Depth of tank	14	meter			
Ballast weight	323057	tonne			

Table 2 Material properties for truss pontoon MOB platform for a single module

Description of material	Values
Elastic modulus	15 GPa
Poisson's ratio	0.3
Nominal plate thickness	0.05 m
Density of top deck	$15.375 \times 10^3 \text{ kg/m}^3$
Density of bottom hull	$11.187 \times 10^3 \text{ kg/m}^3$

3. Numerical analysis

3.1 Numerical analysis module in HYDRAN-XR

HYDRAN-XR* is a computer program used for the three-dimensional linear hydroelastic response analysis of floating and fixed offshore structures. It is designed to analyse the wave induced response of elastic body (flexible structure). Here the eigenvalue problem is solved first to get the mode-shapes, dry natural periods based on the reduced-basis approach. Next the boundary value problem with the mode shapes is solved to find hydrodynamic and hydroelastic responses of the body. The hydrodynamic motion response of a single rigid body and multiple rigid bodies is treated as subsets for general formulation of flexible structures. The theory underlying HYDRAN-XR includes linear hydroelasticity (3D-linear potential theory), linear structural dynamics, and frequency domain solutions (Riggs 2016). These methods consist of constant panel Green function formulation, which is used for the fluid and 3-D shell finite element model for the structure. In HYDRAN-XR mechanical property details like nodes, panel and Poisson's ratio, young's modulus, shear modulus, thickness of plate, density, wave characteristics and water depth are given as input files. In order to analysis using connectors and mooring lines, the location details, axial stiffness, mooring line properties and stiffness are to be included in Input files (Riggs 2016). The output file consists of transfer function or Response Amplitude Operators, modes shape, displacement, stresses, wave excitation forces, added mass matrix, damping matrix, Froude Krylov forces, diffraction forces, dry and wet natural periods.

3.2 Numerical model procedure in HYDRAN-XR

The fluid is assumed to be incompressible and inviscid, the flow is assumed to be irrotational, and linear potential theory is used for analysis. Reduced-basis approach is used for the hydroelasticity solution; especially, in air (dry) normal modes of vibration and are used to calculate the hydroelastic responses (Bishop and Price 1976, Riggs *et al.* 2007, 2008). Dry natural frequencies and eigenvectors are first calculated. Then, the hydrostatic stiffness for flexible structures was determined based on the formulation given in Riggs *et al.* (2008). This formulation includes both the stiffness effect of fluid and the structural geometric stiffness. Geometric stiffness is based on the internal structural forces when the structure is at rest in a calm fluid subject only to gravity and hydrostatic loads, which is obtained by iteration using linear static analysis. Iteration is necessary because the static analysis includes the hydrostatic stiffness, which is required for the calculation of internal forces. In both cases, the structures are freely floating in seawater of infinite depth.

The fluid model is based on the linear potential theory. Linear diffraction radiation wave theory is applicable for large bodies whose characteristic dimension is greater than 0.2 times wave length and also the ratio of wave height to structure diameter is less than one. For these bodies the waves diffract and the flow does not separate around the body and potential theory is employed for the formulation. The incident wave gets diffracted and radiated because of the floating body and hence the theory aims to solve the boundary value problem for these potentials. Due to certain relationships ultimately it is enough to solve only either of diffracted and radiation wave potentials, besides the incident wave potential. The excitation force on the body is calculated based on the incident wave and diffracted wave potentials and the radiated wave potentials yields the added mass and damping. The plan view of global coordinates with wave angle β for single module of truss pontoon MOB platform is shown in Fig. 2, which define the degrees of freedom (DOF) for single module. The coordinate system provided follows module coordinate system $x_1 - x_2 - x_3 (x, y, z)$, where the origin of the coordinate system is located at the centre of gravity (CG) of a single module. The axis x_3 is directed vertically up, axis x_1 is directed along the longitudinal direction of the module and x_2 follows from the right-hand rule. The wave heading angle is denoted by β . Motions in the x_1, x_2 and x_3 directions correspond to surge, sway, and heave motions respectively. Rotation about these axes correspond to roll, pitch and yaw motions. Wave angle of 0° corresponds to following seas. The wave-induced response is determined for wave periods between 2s and 25.5s. Based on the above assumptions, the equations of motion in the frequency domain can be obtained as (Riggs *et al.* 2008).

$$\left[-\omega^2 (M_s^* + M_f^*) + i(C_s^* + \omega C_f^*) + (K_s^* + K_f^*) \right] p = F_w^*, \tag{1}$$

In which $M_s^* = \psi^T M_s \psi$, $K_s^* = \psi^T K_s \psi$ and $K_f^* = \psi^T K_f \psi$, where M_s^* , K_s^* and K_f^* refer to $Q \times Q$ generalized structural mass, stiffness, and hydrostatic stiffness matrices, respectively, C_s^* is the diagonal matrix of hysteretic damping coefficients. M_s^* and K_s^* are also diagonal matrices. F_w^* refers to wave exciting forces, Q is the number of modes; the subscripts s and f denote

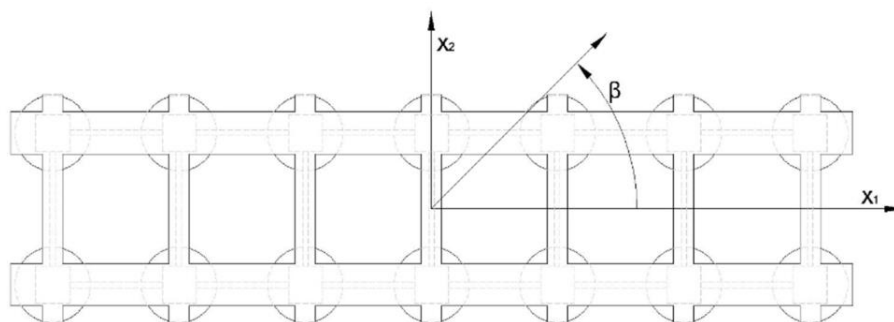


Fig. 2 Plan view of global coordinates with wave angle β for single module

structural and fluid-related quantities respectively; p is vector of the generalized displacements; and the term $e^{i\omega t}$ has been eliminated from both sides of the equations. The actual displacement can be obtained from $u = \psi p$, where u is the $N (< Q)$ vector of displacements, ψ is the $N \times Q$ matrix of assumed normal mode shapes.

3.2.1 Hydrodynamic model

The truss pontoon MOB is considered freely floating in deep water and is based on linear potential theory. The fluid motion is assumed to be small and time harmonic. The total velocity potential as a function of position and structural displacement u is of the form

$$\phi = [\phi_I + \phi_D + i\omega\phi_R u] e^{i\omega t} \quad (2)$$

where ϕ_I , ϕ_D and ϕ_R are the incident, diffracted and radiated potentials satisfies the governing equation in the fluid domain along with the free-surface and bottom boundary condition given by

$$\nabla^2 \phi = 0, \quad (3)$$

$$-\omega^2 \phi + g \frac{\partial \phi}{\partial x_3} = 0 \quad \text{on } x_3 = 0, \quad (4)$$

$$\frac{\partial \phi}{\partial x_3} = 0 \quad \text{for } x_3 \rightarrow \infty, \quad (5)$$

The velocity potential satisfies the radiation condition on the free surface for all the rigid and elastic modes and on the wetted body surface S the diffracted potential satisfies

$$\frac{\partial \phi_D}{\partial n} = \frac{\partial \phi_I}{\partial n} \quad \text{on } S, \quad (6)$$

where n is the outward drawn normal to the wetted surface and the radiation potential satisfy

$$\frac{\partial \phi_R}{\partial n} = n^* \quad \text{on } S, \quad (7)$$

where n^* is the normal displacement of the body. The relationship between the velocity and the pressure is used to determine the dynamic pressure on the structure after the determination of the velocity potential is given by

$$p_r = -\rho \frac{\partial \phi}{\partial t}. \quad (8)$$

The terms in the wave excitation forces in Eq. (1) is obtained from the relation

$$F_{wj}^* = i\rho\omega \int (\phi_I + \phi_D) n_j^* dS, \quad (9)$$

and the terms in M_f^* and K_f^* are given respectively by

$$\mu_{ij} = \rho \Re \int_S \phi_{Ri} n_j^* dS, \quad (10)$$

$$\lambda_{ij} = -\rho \omega \Im \int_S \phi_{Ri} n_j^* dS, \quad (11)$$

Where \Re and \Im refer to the real and imaginary parts respectively, $n_j^*, j = 1, 2, \dots, 6$ are rigid modes and $j = 7, 8 \dots 18$ are elastic modes (Chakrabarti 1987).

3.3 Finite element mesh generation

The finite element model of the truss pontoon VLFS used for the numerical analysis in HYDRAN-XR is shown in Fig. 3. The nineteen connecting trusses are idealized with pipe strut structure at the centre location of the truss frame and these are connected between the columns as shown in Fig. 3. Finite element mesh generation for complex domains is a complex task; the standard pre-processor PATRAN (2012) has been employed. The PATRAN code facilitates bandwidth optimization, which would reduce both computer storage requirements and computation time. The PATRAN data is adapted to conform the element numbering conventions of the HYDRAN-XR. Unique indices are assigned to finite element faces in contact with the free surface and body surface boundary. These face codes/indices are useful for evaluating the element property matrices including the load vector. The finite element models consists of 16252, four node rectangular shell elements and 16202 nodes were used in this analysis. The details of the elements used for different parts of the truss pontoon MOB is given in Table 3. Hydrodynamic mesh consists of rectangular panels, and a one-to-one mapping between structural elements and fluid panels. That is each wetted shell element corresponds one-to-one to a fluid panel element. The fluid panel requires the structural displacement at the middle of the panel, which corresponds to the displacement of the interior structural node. The structural model rectangular element is used to form the five nodes quadrilateral macro-element. The out-of-plane bending is based on shear-deformable Mindlin theory and a constant strain formulation for the in-plane bending. The stiffness comprises of geometric stiffness and hydrostatic stiffness. The geometric stiffness depends on the internal stresses obtained when the structure is in calm water. The hydrostatic stiffness depends on the fluid pressures besides the structural geometric stiffness (Riggs *et al.* 2008).

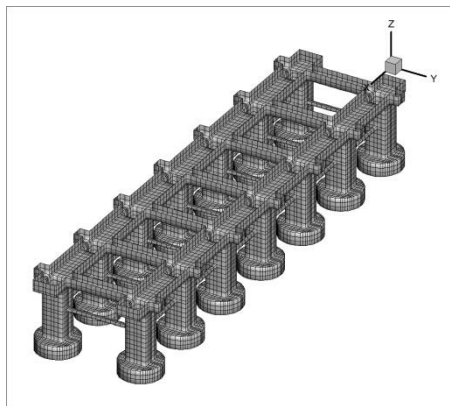


Fig. 3 View of idealized HYDRAN model of truss pontoon MOB - Isometric view

Table 3 Description of the element details of truss pontoon MOB platform of a single module

Description	No. of Nodes	No. of elements	No. of items	Total Nodes	Total elements
Keel tank (bottom hull)	502	490	14	7028	6860
Column	286	261	14	4004	3654
Longitudinal tubular pontoon	44	40	12	528	480
Transverse tubular pontoon	84	78	7	588	546
Longitudinal beam	2030	1890	2	4060	3780
Transverse beam	294	264	7	2058	1848

4. Results and discussion

The numerical analysis is carried out on the truss pontoon MOB using HYDRAN-XR which yields the rigid body modes and deformational modes. The analysis is performed for different dry natural modes, elastic and hydrostatic stiffness, forces and responses of the deformable and rigid bodies.

4.1 Natural period and modes

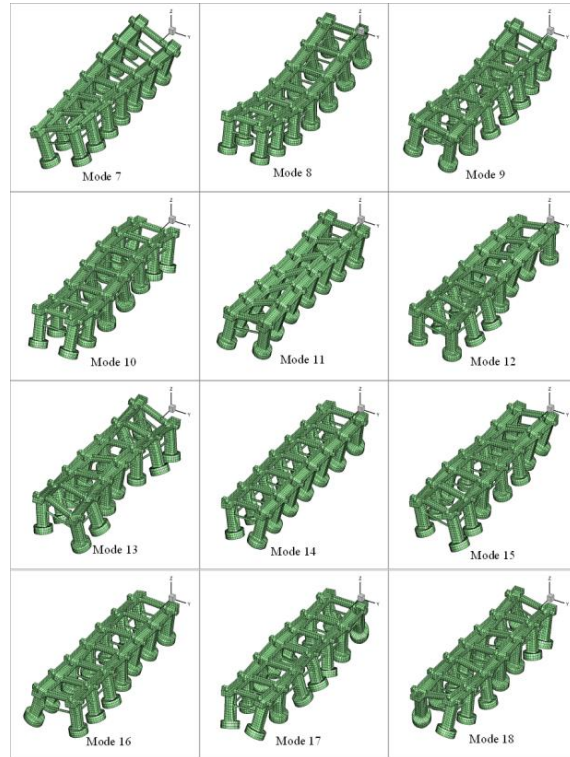
Natural periods in dry and wet conditions are obtained using HYDRAN-XR. The dry natural modes are categorized as rigid and flexible or deformational modes. The modes 1-6 correspond to dry rigid body modes and represent the six degrees of freedom namely the surge, sway, heave, roll, pitch and yaw and these dry natural frequencies are zero. The modes 7-18 corresponds to additional generalized modes due to the flexibility of the body and the details of these flexible or deformational modes and their corresponding natural frequencies are presented in Table 4. The dry and wet mode shapes are shown in Figs. 4(a) and 4(b) and it is observed that the mode shapes are similar to freely floating structure. For dry modes, the deformational modes 7 is purely torsional, and modes 8, 10 are purely vertical bending modes and other modes are mostly torsional or combination of vertical, horizontal and torsional modes. For wet modes, the deformational mode 8 is purely bending and other modes are combination of bending and torsional modes. The wave induced motions of the truss pontoon MOB are obtained from a subset of the dry normal modes to form a reduced basis. The wet natural periods and modes falling in the wave excitation ranges 2-25 s (seconds) were obtained with error less than 1% and are given in Table 5. Comparison of dry natural periods and modes for truss pontoon MOB for some deformational modes (error less than 1%) is given in Table 6. The error here is computed as $\frac{\omega - \omega_n}{\omega} \times 100$, where ω_n is the wet natural frequency and ω is the wave frequency. Comparing the natural periods of wet mode and dry mode it can be seen that three modes namely 7, 8 and 9 have wet natural periods higher than dry natural periods. For these cases it can be observed that the added masses are mostly positive. For modes 13, 14, 15, 16 the dry natural periods are higher than wet natural periods. For these cases it can be observed that the added masses are negative. The combination of increased magnitude of stiffness and positive and negative added masses determines which of the natural periods (dry/wet) is higher.

Table 4 Dry natural periods and modes for truss pontoon MOB

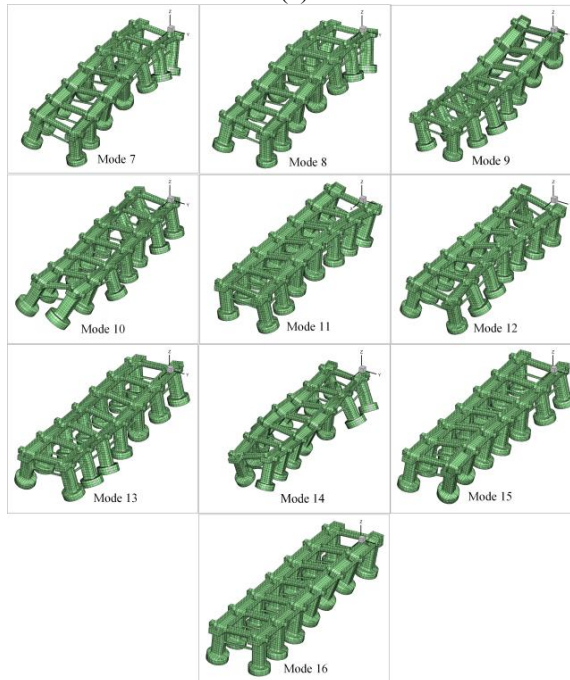
Dry Mode No.	Natural period (s)	Description
7	12.00	Torsion 1
8	11.83	Vertical bending 1
9	6.29	Combination of bending & torsion 1
10	5.31	Vertical bending 2
11	5.09	Combination of bending & torsion 2
12	4.97	Combination of bending & torsion 3
13	4.56	Combination of bending & torsion 4
14	4.24	Combination of bending & torsion 5
15	4.03	Combination of bending & torsion 6
16	4.00	Combination of bending & torsion 7
17	3.88	Combination of bending & torsion 8
18	3.69	Combination of bending & torsion 9

Table 5 Wet natural periods and modes

Modes	Wet natural periods (s)	Error <1%	Description of wet mode (bending & torsion)
7	26.43	0.265	Combination 1
8	18.43	0.409	Vertical bending 1
9	12.94	0.468	Combination 3
10	6.3	0.136	Combination 4
11	5.28	0.446	Combination 5
12	4.99	0.132	Combination 6
13	4.38	0.666	Combination 7
14	3.89	0.335	Combination 8
15	2.39	0.425	Combination 9
16	2.19	0.668	Combination 10



(a)



(b)

Fig. 4 Dry (a) and Wet (b) mode shapes for truss pontoon MOB

Table 6 Comparison of dry and wet natural periods

Modes	Dry natural period (s)	Wet natural periods (s)
7	12.00	26.43
8	11.83	18.43
9	6.29	12.94
10	5.31	6.3
11	5.09	5.28
12	4.97	4.99
13	4.56	4.38
14	4.24	3.89
15	4.03	2.39
16	4.00	2.19

4.2 Elastic and hydrostatic stiffness

In the case of a freely floating structure the restoring forces exist only in modes 3-5 namely heave, roll and pitch. So for modes 3-5, the only contribution for the freely floating structure is the hydrostatic stiffness. For the analysis of the large floating structure the elastic stiffness are also considered along with the hydrostatic stiffness for the deformational modes. Hydrostatic stiffness includes both stiffness effect of the fluid and structural geometric stiffness. Elastic stiffness here refers to material structural stiffness (the bending stiffness EI). In Table 7 the elastic stiffness and hydrostatic stiffness for the modes 7-18 along with the percentage of elastic is presented for deformational modes. Since the modes have been mass normalized the elastic stiffness represents square of the natural frequencies as discussed in Riggs *et al.* (2007). It is observed that the contribution of elastic stiffness is less than 6.5 % for modes 7-18, except for mode 13, where it is about 11% and this is not the case for a barge wherein elastic stiffness contributions are of the same order for lower deformational modes and less than one percent for higher modes (Riggs *et al.* 2007).

4.2.1 Added mass coefficient

The added mass for rigid modes is shown in Figs. 5(a) and 5(b) which corresponds to the linear and rotational modes of a rigid body. For the deformational modes the added mass moment of inertia for modes 7-18 are shown in Figs. 5(c)-5(f). It can be observed that for the rigid body modes the added mass values are positive and mass moment of inertia values are in the order of 10^{12} . For mode 7 the values are about $1/1000^{\text{th}}$ of rigid modes (roll, pitch and yaw) and the modes above 10 exhibit negative values with the highest negative mass moment of inertia is observed for mode 18. In the deformational modes for most of them the negative value indicates less fluid resistance in these modes and hence for a given excitation the motion contribution by these modes is relatively significant.

Table 7 Generalized Diagonal Stiffness Coefficients for truss pontoon MOB

Dry Mode no.	Elastic	Hydrostatic	% Elastic
7	0.274	15.30	1.790
8	0.282	9.380	3.006
9	0.997	54.30	1.836
10	1.40	22.80	6.140
11	1.530	43.50	3.517
12	1.60	33.70	4.747
13	1.90	17.51	10.850
14	2.20	82.40	2.669
15	2.44	80.30	3.038
16	2.46	96.30	2.554
17	2.62	56.0	4.678
18	2.88	45.0	6.40

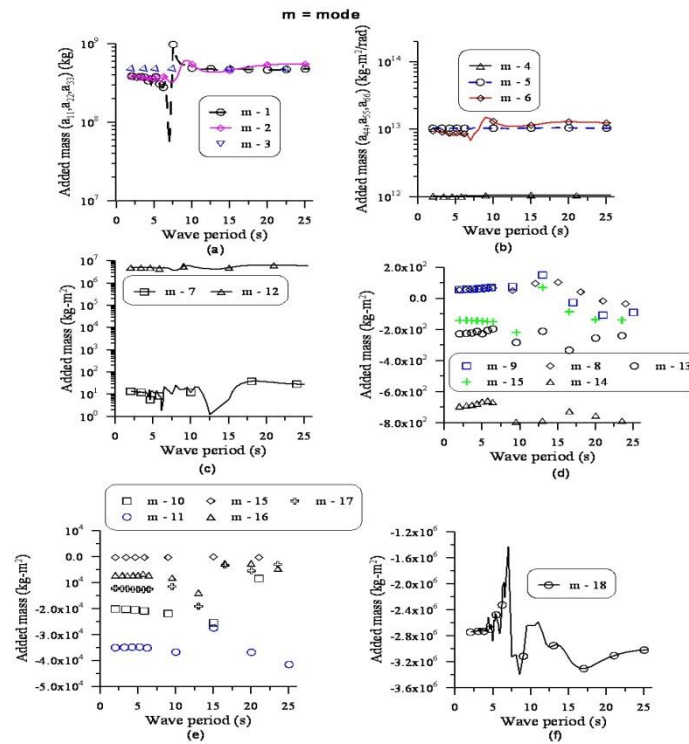


Fig. 5 Added mass coefficient for truss pontoon MOB

4.2.2 Damping coefficient

The damping coefficient values for rigid modes is shown in Figs. 6(a) and 6(b) which corresponds to the linear and rotational modes of a rigid body and are all positive values exhibiting loss of energy in motion. For the deformational modes the damping moment are positive as well as negative and for some modes the values are mostly negative for different wave periods. The negative damping values indicate that for these modes and periods there is no fluid resistance for the body, thereby increasing the response of the body. Strong frequency dependency is observed for modes 7-18 as shown in Figs. 6(c)-6(e).

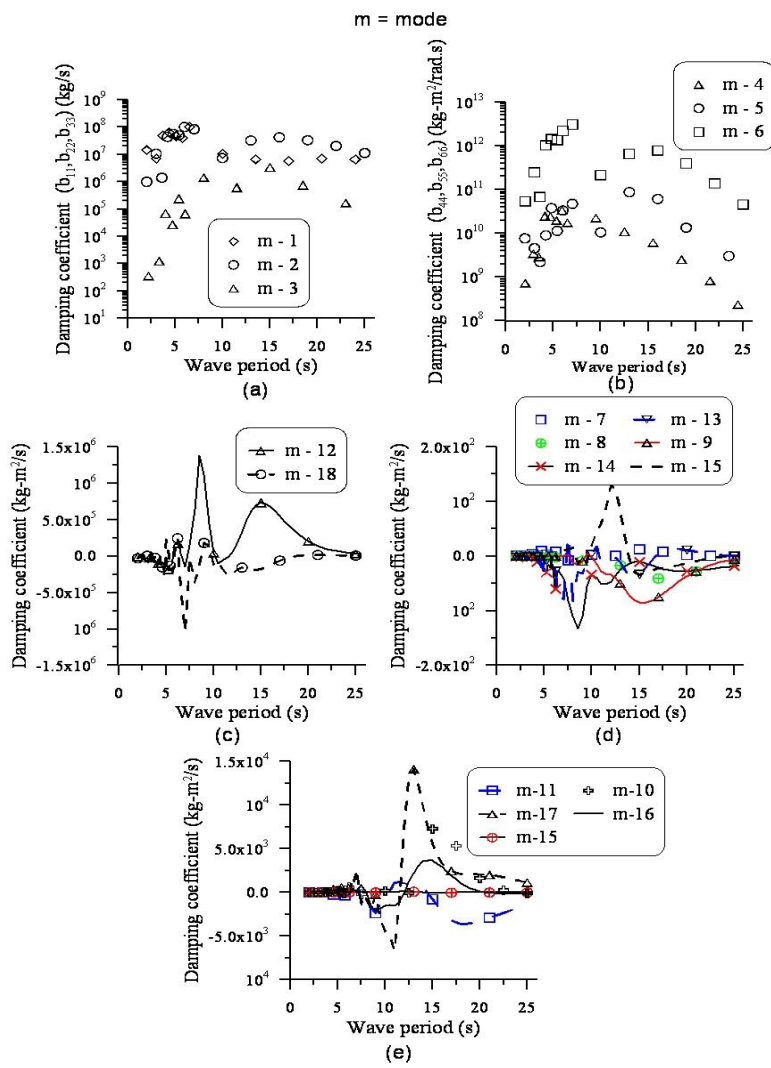


Fig. 6 Damping coefficient for truss pontoon MOB

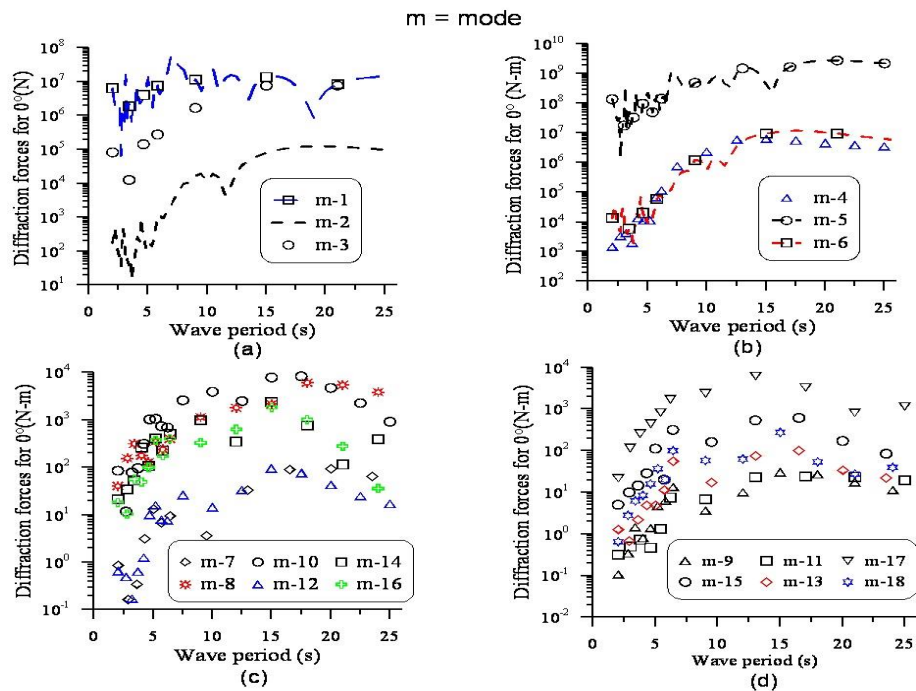


Fig. 7 Diffraction forces for 0° wave heading angle of truss pontoon MOB

4.2.3 Diffraction force

The presence of large body in waves diffracts waves and one component of wave excitation force is due to the diffraction force. In Figs. 7(a) and 7(b), the diffraction force for the rigid body modes is presented and it is observed that, the diffraction force increases with wave period and the diffraction force in the surge and heave direction are higher than that of sway direction for 0° wave heading angle. The diffraction moment shows an increasing trend as the wave periods increase. The pitch exciting moment is higher of the order four as compared to surge and yaw exciting moment. The diffraction moment for deformational modes are shown in Figs. 7(c) and 7(d) and it can be observed that for the mode7 and mode 9, the diffraction force are close to zero for wave period below 15 s. Significant variation in the moment are observed for mode 8, 10 and 18. This suggests that, the nature of bending and twisting has a pronounced effect on the diffraction forces.

4.2.4 Froude Krylov force

The Froude-Krylov force is due to incident waves and these forces and moment for the rigid body modes are shown in Figs. 8(a)-8(d) It is easy to observe that the sway forces are small and close to zero, especially for wave periods below 8 seconds. The surge force is greater than the sway force for wave periods below 17 s and these forces are of same order for higher wave periods. The pitch exciting moment dominates over the roll and yaw exciting moments as seen from Fig. 8(b) and for the deformational modes, these moments are small and close to zero for modes 7, 9, 11 and 12. Significant variations in the moment are contributed by modes 8, 10, 15 and 17 as shown in 8(c)-8(d).

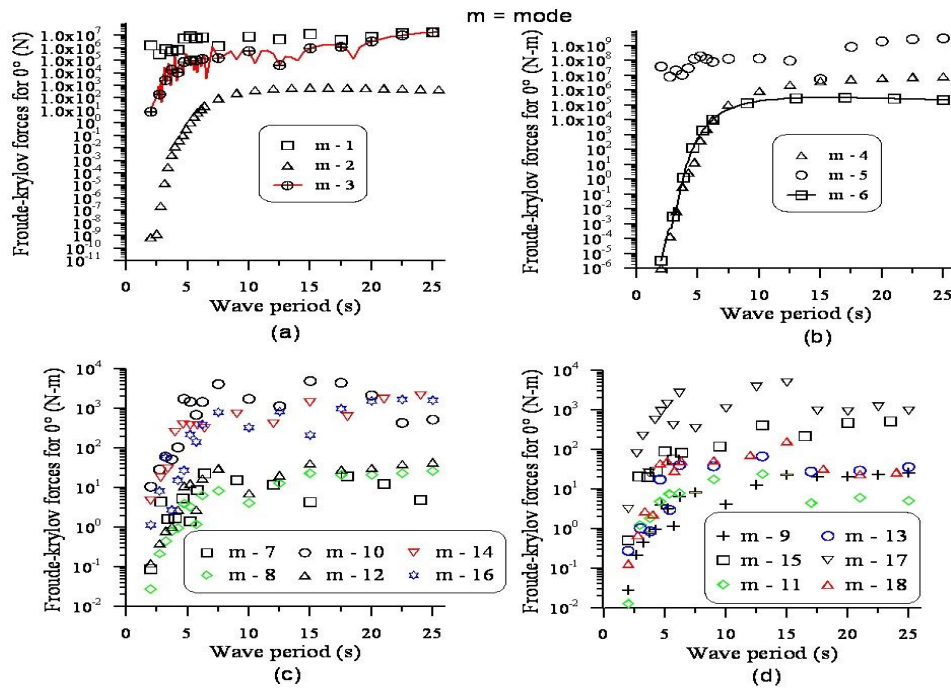


Fig. 8 Froude-Krylov forces for 0° wave heading angle of truss pontoon MOB

4.2.5 Excitation force

The sum of diffraction and Froude-Krylov force/moment forms the excitation forces. The variation of the excitation forces and moment for the rigid body modes are shown in Figs. 9(a)-9(d). The sway excitation forces are very less for smaller wave periods. The surge excitation force is greater than the heave excitation force for the zero heading angle. The pitch exciting moment is higher than the other excitation moments as expected. For the deformational modes, the excitation moment is of the order 10^4 , less than that of rigid body modes. In fact the moment is close to zero for modes, 7, 11 and 12. Significant variation in the moments is contributed by the deformable modes 7, 10, 15 and 17.

4.2.6 Response Amplitude Operators RAOs

The wave induced response for the rigid body modes in terms of Response Amplitude Operators (RAO= structure response /wave amplitude) are shown in Figs. 10(a) and 10(b) in the case of 0° wave heading angle for surge, sway and heave mode. The surge response is higher as compared to sway response and it is observed that, there is an increasing trend in the response for truss pontoon mobile offshore base. The rotational modes peak value at pitch is 0.3 deg/m and other modes are less than 0.1deg/m which is three times lesser than pitch values for 0° heading wave angles as shown in Fig. 10(b). Fig. 10(c) shows the validations of heave RAO obtained using HYDRAN-XR with that of existing experimental results of rigid body MOB reported in Srinivasan and Sundaravadivelu (2013). The error in the values near the natural period suggests that additional damping has to be included in the model. In the case of deformational modes, the

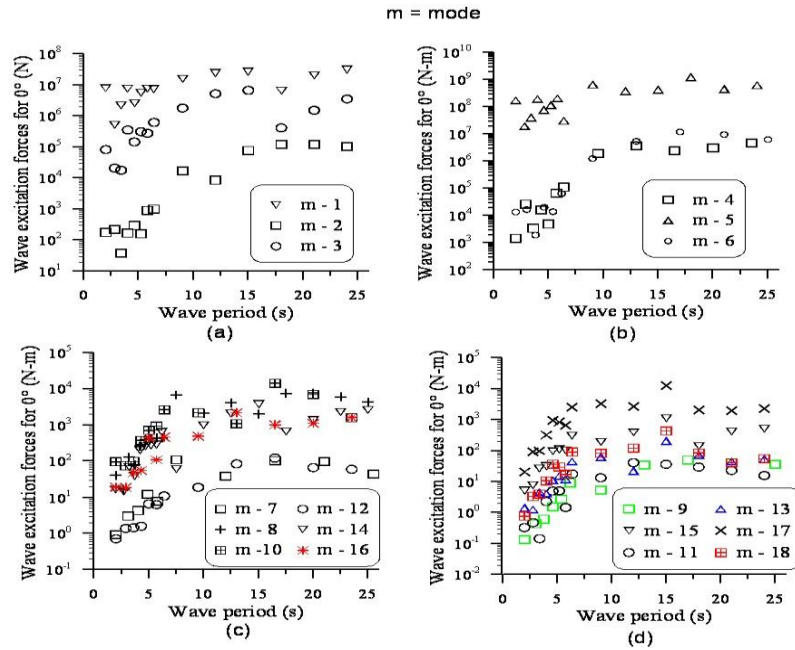


Fig. 9 Wave excitation forces for 0° wave heading angle of truss pontoon MOB

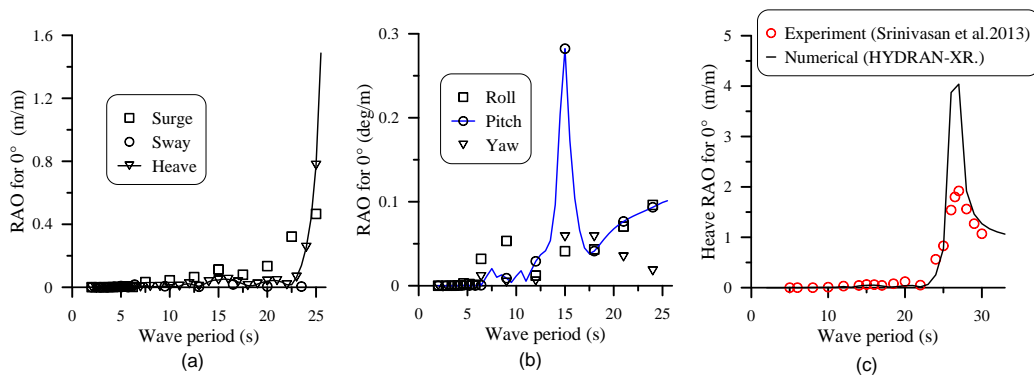


Fig. 10 RAOs of translation, rotation of truss pontoon MOB for 0° wave heading angle

bending moment RAOs are shown in Figs. 11(a) and 11(b) for 0° wave heading angle. The bending moment for most of the modes peaks near wave period of 15 s and for mode-12 and mode-13 peak values are $4.0 \times 10^3 \text{ N-m/m}$ and $1.2 \times 10^3 \text{ N-m/m}$ respectively. The coupled amplification of mode 12 and 13 with pitch at secondary peak of 15 s is attributed to the significant off diagonal modal mass values i.e., $m(5, 12)$, $m(5, 13)$. These deformable bending moments are combination of bending and torsion as well as wave characterises.

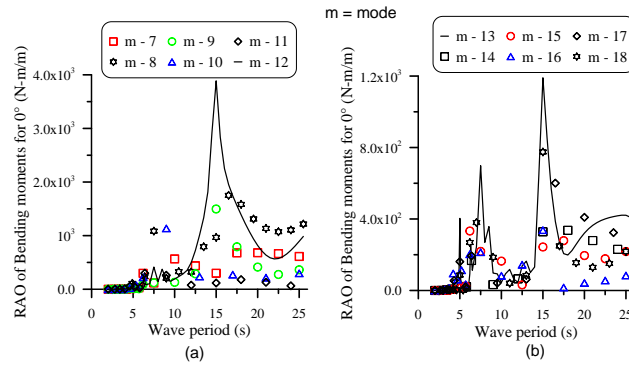


Fig. 11 RAOs of Bending moment for deformational modes of truss pontoon MOB for 0° wave heading angle

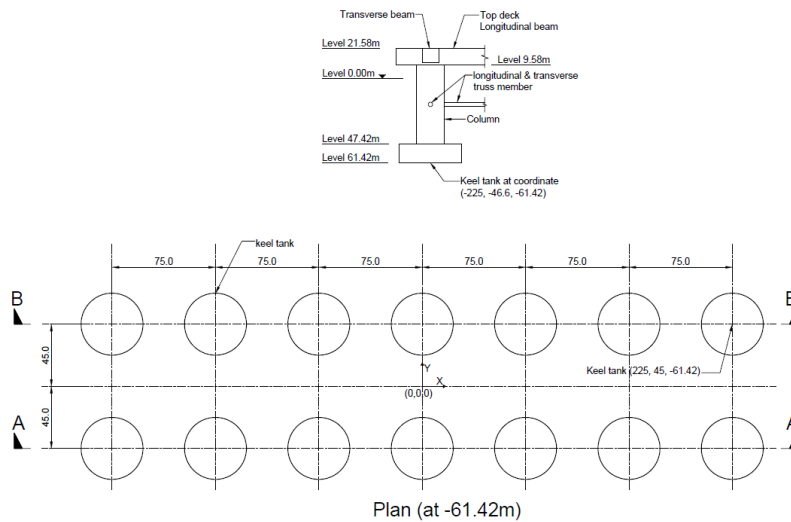


Fig. 12 View the nodal points of truss pontoon MOB

4.2.7 Vertical displacement

The vertical displacements are obtained for the nodal points shown in Fig. 12, which are centre of keel tanks. The vertical displacements for these nodal points by considering the body as ‘hydroelastic’ and ‘rigid’ are compared in Figs. 13(a)-13(n) for 0° wave heading angle for fourteen different nodal points. From these graphs it can be seen that the rigid body responses are lower compared to elastic body in most of the wave periods in the range of 5-20 s. Hence it is concluded that the vertical displacement of the rigid body assumption underestimates the vertical displacements. On the other hand for higher wave periods the vertical displacement for both rigid and elastic body increases. Table 8 compares the values of peak vertical displacements along sections AA and BB at the nodal points for elastic body and rigid body.

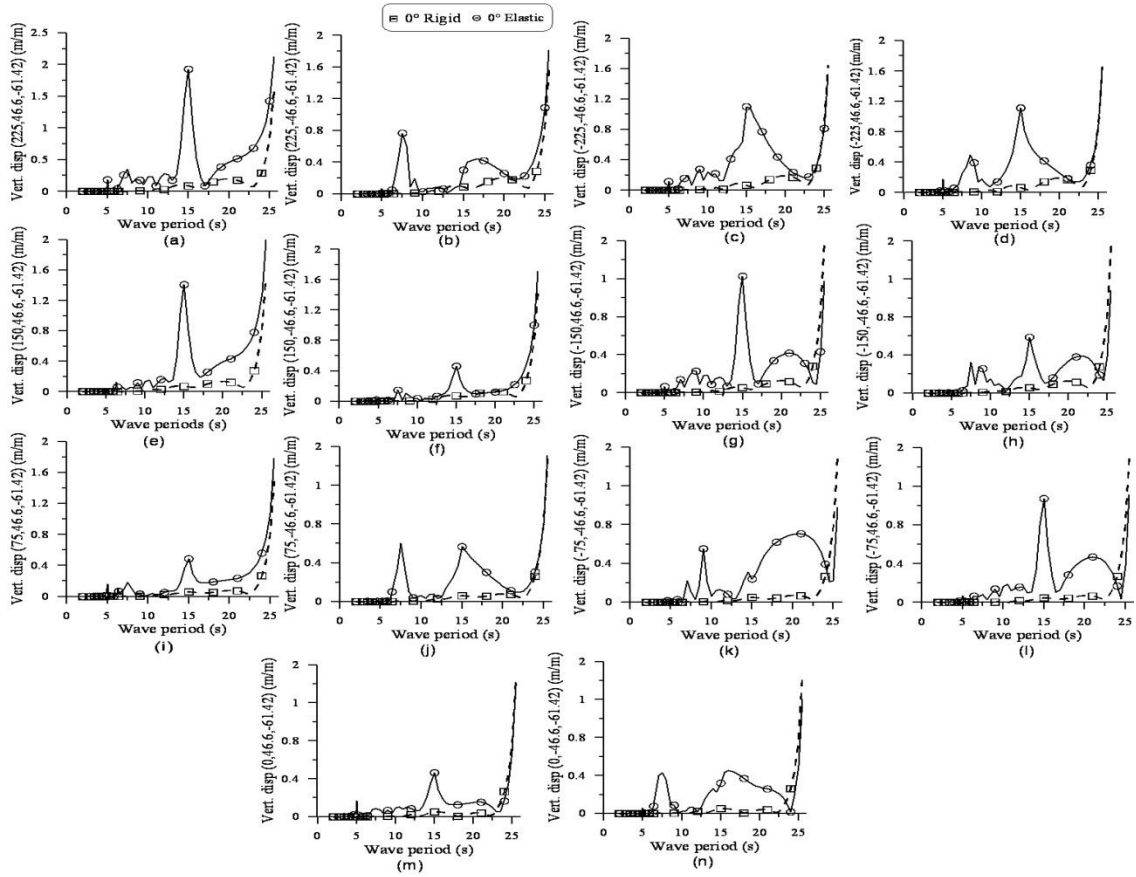


Fig. 13 Comparison of vertical displacement of rigid and elastic body

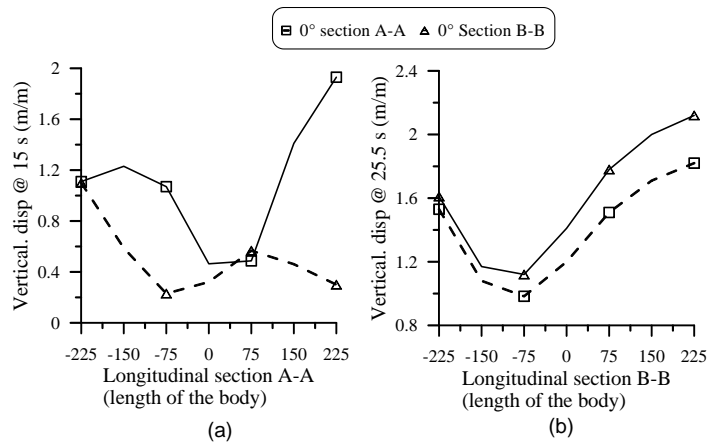


Fig. 14 Peak value of vertical displacement of the truss pontoon MOB

Table 8 Peak Displacement Comparison of rigid body and elastic body of truss pontoon MOB

Description	Rigid body (m/m)		Elastic body (m/m)		
	Section	BB	Section AA	Section BB	Section AA
At Centre of bottom keel tank	1.5		1.5	1.42	1.1
From origin of the right corner x-axis	1.5		1.55	2.2	1.82
From origin of the left corner x-axis	1.65		1.6	1.61	1.53
From x-axis coordinates at (150, 46.6, -61.42)	1.5		1.6	2	1.71
From x-axis coordinates at (-150, 46.6, -61.42)	1.9		1.9	1.17	1.1
From x-axis coordinates at (75, 46.6, -61.42)	1.5		1.5	1.78	1.51
From x-axis coordinates at (-75, 46.6, -61.42)	1.6		1.6	1.12	0.98

The vertical displacement profile of the truss pontoon MOB for two wave periods, 15 s and 25.5 s, wherein the vertical displacements are maximum, are shown in Figs. 14(a) and 14(b). These are plotted along the longitudinal direction on either side of the truss pontoon MOB and combinational effects on bending and torsion along the longitudinal section is discussed. Fig. 14(a) shows the displacement of the truss pontoon MOB are asymmetric at the wave period 15 s and the model slightly tilt from the section A-A to section B-B at wave period 25.5 s. Considering a wave of 30 m this corresponds to a maximum displacement of about 60 m at one end of the truss pontoon in severe seas in isolated model. However these displacements vary in multi-module case and if necessary dampers have to be installed to reduce vertical displacements.

The rotation about x-axis of is shown in Figs. 15(a)-15(g) for 0° wave heading angle for different nodal points along the centreline, in longitudinal direction at the top deck level. The rotation about x-axis is of almost same order for different nodal point but it is observed less for lower wave periods. The rotation about y-axis is shown in Figs. 16(a)-16(g) for 0° wave heading angle. The rotation about y-axis increases with wave period. The nodal point rotation about y-axis is same order as that of the x-axis rotation. The rotations are less than one degree for unit wave height. The maximum longitudinal stresses in entire region except top deck of truss pontoon MOB is shown in Fig. 17 for 0° wave heading angle. It is observed that the longitudinal stress variation is above 1.0×10^4 Mpa/m for most of the regions and very less near the far end (rear) of the MOB. Further, the maximum longitudinal stresses in top deck of truss pontoon MOB is shown in Fig.18 for 0° wave heading angle. The variation in the maximum longitudinal stress in the top deck is observed in the middle portion of the top deck. A comparison of the performance of the truss pontoon MOB with that of a barge whose length is 100 m and width and draft are one order smaller, analysed by Riggs *et al.* (2007) is shown in Table 9.

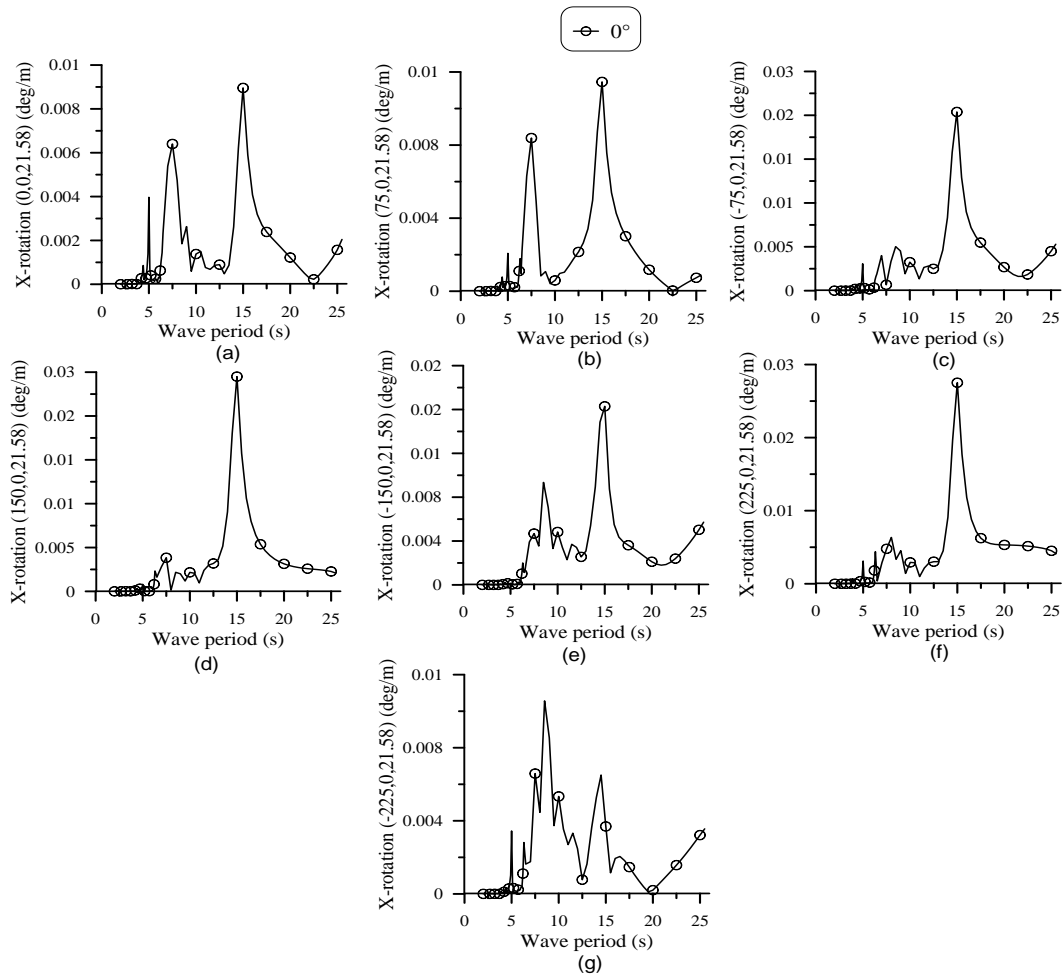


Fig. 15 X-rotation of truss pontoon MOB

Table 9 Comparison of barge (100×10×2 m draft 1 m) and truss pontoon MOB (500×135×83 draft 61.42 m)

Si no.	Description	Barge (Riggs et al.2007)	Truss pontoon MOB
1	Heave RAO maximum	1.1 (m/m) (at peak)	1.4 (m/m) (up to 25.5 sec)
2	Generalized Diagonal elastic stiffness coefficient	7.78 & 978 (max. & min.)	0.274 & 2.88 (max. & min.)
3	Vertical displacement at mid-ships for flexible	1.0 (m/m)	0.9 (m/m)
4	Vertical displacement at edge	1.3 (m/m)	2.2 (m/m)
5	Longitudinal stress	18 (Mpa/m) (at Center of top deck)	10 (Mpa/m)

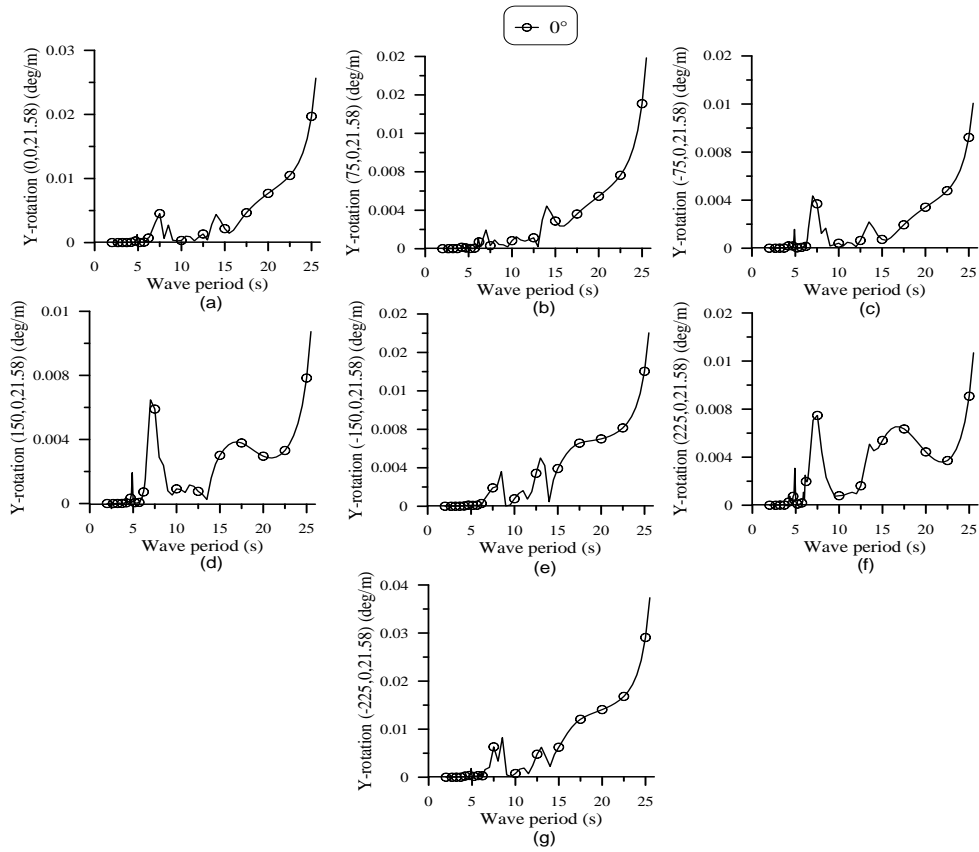


Fig. 16 Y-rotation of truss pontoon MOB

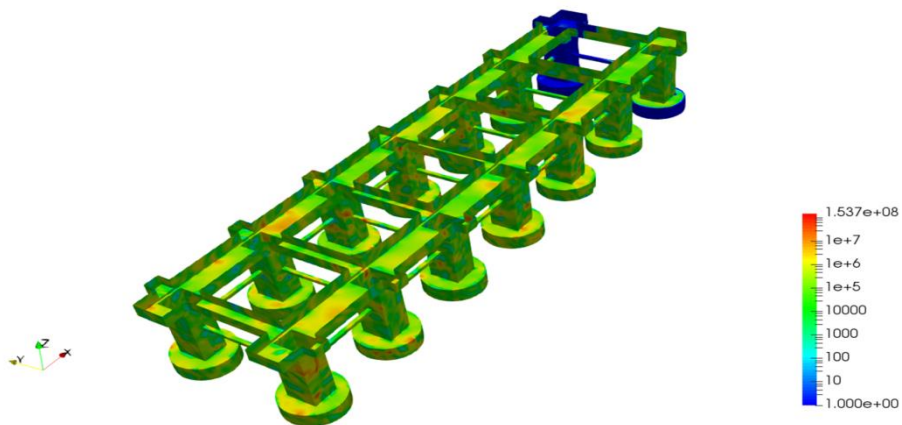


Fig. 17 Maximum longitudinal stresses in entire region except top deck of truss pontoon MOB for 0° wave angle (values in MPa/m)

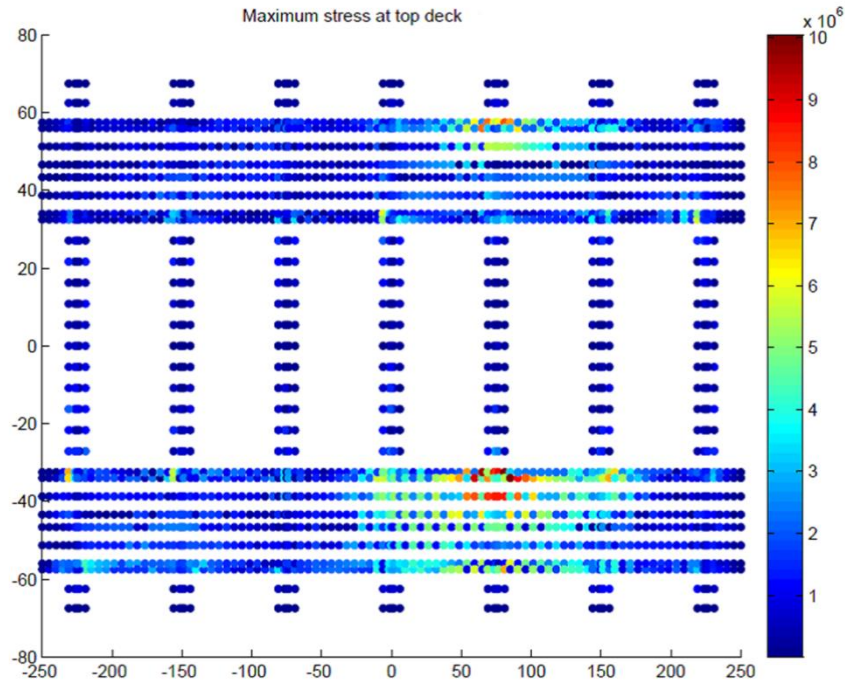


Fig. 18 Maximum longitudinal stresses in top deck of truss pontoon MOB for 0° wave angle (values in MPa/m)

5. Conclusions

This paper presents hydroelastic analysis carried out on an innovative VLFS called truss pontoon Mobile Offshore Base (MOB) platform concept proposed by Srinivasan and Sundaravadivelu (2013). The MOB is modelled and hydroelastic analysis is carried out using HYDRAN-XR* for regular 0° waves heading angle. Results are presented for variation of added mass and damping coefficients, diffraction and wave excitation forces, RAOs for translational, rotational and deformational modes and vertical displacement at salient sections, rotations along longitudinal and transverse directions for wave periods ranging from 2- 25 s. Peak stresses and bending moment for the entire structures are also obtained. Comparison of rigid body and elastic body of nodal vertical displacement brings out the importance of hydroelastic analysis of the structure wherein the displacements predicted are higher. This study helps in performance evaluation of the truss pontoon VLFS in different sea conditions and further adopt design modifications for safe utility. Further analysis has to be carried out for multi body case and validate the numerical studies using experimental measurements on a scaled elastic truss pontoon MOB.

Acknowledgements

The authors would like to acknowledge IIT Madras for supporting financially to perform the research work and also thank Prof. H. Ronald Riggs, University of Hawaii at Manoa, for providing valuable insights in HYDRAN-XR*.

References

- Barrientos, M.A., Gatica, G.N., Rodríguez, R. and Torrejón, M.E. (2004), “Analysis of a coupled BEM/FEM Eigen solver for the hydroelastic vibrations problem”, *ESAIM: Math. Model. Numer. Anal.*, **38**(4), 653-672.
- Bishop, R.E.D. and Price, W.G. (1976), “On the relationship Between Dry modes and Wet modes in the theory of ship Response”, *J. Sound Vib.*, **45**(2), 157-164.
- Bishop, R.E.D., Price, W.G. and Wu, Y. (1986), “A general linear hydroelasticity theory of floating structures moving in a seaway”, *Royal Society*, **316**(1538), 375-426
- Chakrabarti, S.K. (1987), *Hydrodynamics of Offshore Structures*, WIT press.
- Huang, L.L. and Riggs, H.R. (2005), “Development of a new interfacing strategy for fluid-structure interaction”, *J. Eng. Maritime Environ.*, **219**, 131-148.
- ISSC.(2006), “Report of specialist Task Committee VI.2, very large floating structures”, (Eds., Frieze, P.A., Sheno, R.A.), *Proceedings of the 16th International Ship and Offshore Structure Congress*, Southampton, UK.
- Kim, B.W., Hong, S.Y., Kyoung, J.H. and Cho, S.K. (2007), “Evaluation of bending moments and shear forces at unit connections of very large floating structures using hydroelastic and rigid body analyses”, *Ocean Eng.*, **34**(11-12), 1668-1679.
- Lee, S.W. and Webster, W.C. (1994), “A preliminary to the design of a hydroelastic model of a floating airport”, *Proceeding of the International Conference on Hydroelasticity in Marine Technology*, Trondheim, Norway.
- Liu, J., Riggs, H.R. and Tessler, A. (2000), “A four-node shear deformable shell element developed via explicit Kirchhoff constraints”, *Int. J. Numer. Meth. Eng.*, **49**, 1065-1086.
- Patran, M.S.C. (2016), User’s Guides and Reference Manuals.
- Pinkster, J.A. and Scholte, E.M. (2001), “The behaviour of a large air-supported MOB at sea”, *Mar. Struct.*, **14**(1-2), 163-179.
- Riggs, H.R. (2016), Hydrodynamic Response Analysis with Integrated Structural Finite Element Analysis, HYDRAN-XR, v 16.3.
- Riggs, H.R. and Ertekin, R.C. (1998), “Impact of connector stiffness on the response of a multi-module mobile offshore base”, *Proceedings of the 8th International Offshore and Polar Engineering Conference*, Montreal, Canada.
- Riggs, H.R. and Ertekin, R.C. (1999), “Response characteristics of serially connected semisubmersibles”, *J. Ship Res.*, **43**(4), 229-240.
- Riggs, H.R., Hideyuki, S., Ertekin, R.C., Jang, W.K. and Iijima, K. (2008), “Comparison of hydroelastic computer codes based on the ISSC VLFS benchmark”, *Ocean Eng.*, **35**, 589-597.
- Riggs, H.R., Niimi, K.M. and Huang, L.L. (2007), “Two benchmark problems for three-dimensional, linear hydroelasticity”, *J. Offshore Mech. Arct.*, **129**, 149-157.
- Srinivasan, N. and Sundaravadivelu, R. (2013), “Ocean space utilization using very large floating semi-submersible”, *Proceedings of the ASME 32nd international Conference on Ocean, Offshore and Arctic Engineering*, Nantes, France.
- Srinivasan, N., Chakrabarti, S. and Radha, R. (2006), “Response analysis of a Truss-Pontoon Semisubmersible with Heave-Plates”, *J. Offshore Mech. Arct.*, **128**.

- Suzuki, H., Yoshida, K. and Iijima, K. (1996), "A consideration of the structural design of a large-scale floating structures", *J. Mar. Sci. Technol.*, **1**, 255-267.
- Tulin, M.P. (1999), "Hydroelastic scaling", *Proceedings of 3th International Workshop on Very Large Floating Structures*, Honolulu, Hawaii, USA.
- Venkataraman, V. (2001), "Dynamic response of a mobile offshore base hydroelastic test model", M.S. dissertation, The university of Maine.
- Wang, C.M. (2015), "Mega floating structures", *Singapore maritime technology conference*, Singapore.
- Wu, Y., Wang, D., Riggs, H.R. and Ertekin, R.C. (1993), "Composite singularity distribution method with application to hydroelasticity", *Mar. Struct.*, **6**, 143-163.
- Zueck, R., Palo, P. and Taylor, T. (1998), "Mobile offshore base", *Proceedings of the 8th International Offshore and Polar Engineering Conference, Montreal, Canada*.

MK